JOURNAL OF AIRCRAFT
Vol. 46, No. 6, November–December 2009

Improved Flutter Boundary Prediction for an Isolated Two-Degree-of-Freedom Airfoil

Jordan B. Schwarz,* Earl H. Dowell,† Jeffrey P. Thomas,‡ and Kenneth C. Hall§
Duke University, Durham, North Carolina 27708-0300
and
Russ D. Rausch¶ and Robert E. Bartels**
NASA Langley Research Center, Hampton, Virginia 23681

DOI: 10.2514/1.30703

A novel method of computing the flutter boundary for an isolated airfoil based on a high-fidelity computational fluid dynamics model reveals unusual behavior in a critical transonic range. Inviscid and viscous predictions of the flutter boundary for the two airfoils examined differ substantially in this critical region and become sensitive to Mach number and grid topology due to complicated shock/boundary-layer interactions. Computational fluid dynamics predictions of the flutter boundary for a NACA 0012 section airfoil are also compared with previous experimental results.

Nomenclature

a	=	nondimensional location of the airfoil elastic axis, e/b
b, c	=	semichord and chord
$\bar{c}_l$, $\bar{c}_m$	=	nondimensional coefficients of lift and moment about the elastic axis for simple harmonic motion
e	=	location of the elastic axis, measured positive aft of the airfoil midchord
g	=	nondimensional coefficient of structural damping
h, $\bar{h}$	=	airfoil plunge displacement and its nondimensional amplitude, $\bar{h} = h/b$
M	=	freestream Mach number
$M_{\text{e.a.}}$	=	moment about the elastic axis
m	=	airfoil sectional mass
q_f	=	flutter dynamic pressure, $\frac{1}{2}\rho U_f^2$
r_α	=	nondimensional radius of gyration of the airfoil about the elastic axis, $r_\alpha^2 = I_\alpha/mb^2$
S_α	=	first moment of inertia about the elastic axis or static unbalance
U	=	freestream velocity
V	=	reduced velocity, $U/\omega_\alpha b$
x_α	=	airfoil static unbalance, S_α/mb
α	=	airfoil pitch angle
μ	=	mass ratio; $m/\pi\rho b^2$
ρ	=	flow density
ω, $\bar{\omega}$	=	frequency and reduced frequency based on airfoil chord, $\bar{\omega} = \omega c/U$
ω_h, ω_α	=	uncoupled natural frequencies of plunge and pitch degrees of freedom

Presented as Paper 1819 at the 49th AIAA/ASME/ASCE/AHS/ASC Structures, Structural Dynamics, and Materials Conference, Schaumburg, IL, 7–10 April 2008; received 27 January 2009; accepted for publication 11 August 2009.

*Graduate Student, Department of Mechanical Engineering and Materials Science; currently Dynamic Concepts, Inc., Huntsville, AL. Young Professional Member AIAA.
†William Holland Hall Professor, Department of Mechanical Engineering and Materials Science. Honorary Fellow AIAA.
‡Research Assistant Professor, Department of Mechanical Engineering and Materials Science. Member AIAA.
§Julian Abele Professor and Chair, Department of Mechanical Engineering and Materials Science. Associate Fellow AIAA.
¶Aerospace Engineer, Aeroelasticity Branch. Member AIAA.
**Senior Aerospace Engineer, Aeroelasticity Branch. Member AIAA

I. Introduction

FLUTTER prediction in transonic flows is of considerable interest to the design of airfoils and aircraft. Researchers at Duke University have created several computational fluid dynamic (CFD) codes using a novel harmonic balance (HB) technique. This new solution method offers reduced computational expense, particularly for flows involving harmonic motion such as those found in flutter and limit cycle oscillation (LCO) prediction.

Kholodar et al. [1] used an inviscid HB flow solver to predict the flutter boundary and LCO for isolated two-degree-of-freedom (2-DOF) airfoils. Their computational flutter analysis showed good correlation with the experimental results of Rivera et al. [2], except in the flow region near $M = 0.9$. This disagreement was hypothesized to be due to the contributions of viscous effects.

Since that time, Thomas et al. [3] developed an HB flow solver using the viscous Navier–Stokes equations and a Spalart–Allmaras turbulence model. In conjunction with a novel method of extracting the flutter condition, this Navier–Stokes flow solver was used to compute the flutter boundary for the NACA 64A010 and NACA 0012 airfoils previously examined by Kholodar et al. [1] to confirm whether viscous effects were responsible for the disagreement between computational and experimental results.

II. Governing Equations

A typical 2-DOF airfoil section can be modeled by the following time-domain equations of motion:

$$m\ddot{h} + S_\alpha\ddot{\alpha} + K_h h = -L, \qquad S_\alpha\ddot{h} + I_\alpha\ddot{\alpha} + K_\alpha\alpha = M_{\text{e.a.}} \tag{1}$$

The left-hand side terms of these equations constitute a linear structural model for the pitch and plunge coordinates of the airfoil. The right-hand terms contain the aerodynamic loads, which are determined via the HB flow solver in this analysis. Hall et al. [4] present an example of the harmonic balance method as applied to inviscid aerodynamics. The extension of this method to viscous cases is discussed by Thomas et al. [3].

The time-domain equations can be recast in the frequency domain in terms of nondimensional variables:

$$\left[-\bar{\omega}^2\begin{pmatrix}1 & x_\alpha\\ x_\alpha & r_\alpha^2\end{pmatrix} + \frac{4}{V^2}\begin{pmatrix}\omega_h^2/\omega_\alpha^2 & 0\\ 0 & r_\alpha^2\end{pmatrix}\right]\begin{Bmatrix}\bar{h}\\ \alpha\end{Bmatrix} = \frac{4}{\pi\mu}\begin{Bmatrix}-\bar{c}_l(\bar{h},\alpha,\bar{\omega})\\ 2\bar{c}_m(\bar{h},\alpha,\bar{\omega})\end{Bmatrix} \tag{2}$$

III. Flutter Analysis Methods

To determine the flutter condition for an airfoil, the HB flow solver is run for very small airfoil motions of $\bar{h}/b = 0.001$ in the pitch degree of freedom and $\bar{\alpha} = 0.001$ in plunge. These motions are small enough that the system response is dynamically linear and a single harmonic is sufficient for modeling the structural motion and aerodynamic flowfield. For small harmonic motions, the aerodynamic terms of Eq. (2) can be written in terms of aerodynamic transfer functions as

$$\frac{4}{\pi\mu}\begin{Bmatrix} -\bar{c}_l(\bar{h},\alpha,\bar{\omega}) \\ 2\bar{c}_m(\bar{h},\alpha,\bar{\omega}) \end{Bmatrix} = \frac{4}{\pi\mu}\begin{pmatrix} -\frac{d\bar{c}_l}{dh} & -\frac{d\bar{c}_l}{d\alpha} \\ 2\frac{d\bar{c}_m}{dh} & 2\frac{d\bar{c}_m}{d\alpha} \end{pmatrix}\begin{Bmatrix} \bar{h} \\ \alpha \end{Bmatrix} \tag{3}$$

where $h/b = \bar{h}e^{i\omega t}$ and $\alpha = \bar{\alpha}e^{i\omega t}$. All terms can then be taken to the left-hand side of Eq. (3), producing the eigenvalue problem:

$$\left[-\bar{\omega}^2\begin{pmatrix} 1 & x_\alpha \\ x_\alpha & r_\alpha^2 \end{pmatrix} + \frac{4}{V^2}\begin{pmatrix} \omega_h^2/\omega_\alpha^2 & 0 \\ 0 & r_\alpha^2 \end{pmatrix} - \frac{4}{\pi\mu}\begin{pmatrix} -\frac{1}{2}\frac{d\bar{c}_l}{dh} & -\frac{1}{2}\frac{d\bar{c}_l}{d\alpha} \\ \frac{d\bar{c}_m}{dh} & \frac{d\bar{c}_m}{d\alpha} \end{pmatrix}\right]\begin{Bmatrix} \bar{h} \\ \alpha \end{Bmatrix} = \begin{Bmatrix} 0 \\ 0 \end{Bmatrix} \tag{4}$$

The determinant of the left-hand side matrix, referred to here as E, must be zero at the flutter onset condition:

$$\det(E) = \left|-\bar{\omega}^2\begin{pmatrix} 1 & x_\alpha \\ x_\alpha & r_\alpha^2 \end{pmatrix} + \frac{4}{V^2}\begin{pmatrix} \omega_h^2/\omega_\alpha^2 & 0 \\ 0 & r_\alpha^2 \end{pmatrix} - \frac{4}{\pi\mu}\begin{pmatrix} -\frac{1}{2}\frac{d\bar{c}_l}{dh} & -\frac{1}{2}\frac{d\bar{c}_l}{d\alpha} \\ \frac{d\bar{c}_m}{dh} & \frac{d\bar{c}_m}{d\alpha} \end{pmatrix}\right| = 0 \tag{5}$$

Because the lift and moment coefficients resulting from harmonic motions are complex, so is the determinant of E. A numerical scheme can be used to find where this determinant is zero. Two schemes were pursued, and Kholodar et al.'s [1] inviscid computational analysis of a NACA 64A010A airfoil was used as a baseline for comparison. This airfoil has structural parameters $x_\alpha = 0.25$, $r_\alpha^2 = 0.75$, and $a = -0.6$.

A. Minimum Magnitude Solution

One approach to solving Eq. (5) is to seek the reduced velocity for which the magnitude of $\det(E)$ (the length of the eigenvector of E) goes to zero. For a given run of the HB flow solver, the reduced frequency of the airfoil motion is specified, as is the Mach number. For fixed M and $\bar{\omega}$, a sweep of values of reduced velocity is conducted. At each V, $\det(E)$ is found. If the correct range of reduced frequency is examined, then in that range should lie the point at which $\det(E)$ goes to zero. A C++ code was written to implement this procedure, and gnuplot was used for visualization of results.

In order for this method to produce meaningful results, the grid of V and $\bar{\omega}$ must be fine enough to capture all of the conditions for which $\det(E)$ goes to zero. It is computationally expensive to run the HB flow solver for all desired $\bar{\omega}$. Instead, a few well-chosen values can be used, and cubic splines can then be fitted to these data.

These computations provide the determinant magnitude as a function of V and $\bar{\omega}$. In the minimum magnitude solution, the minimum value of $\det(E)$ is determined for each value of V and $\bar{\omega}$, and the conditions are obtained for which this result is most nearly zero. One shortcoming of this method is that the magnitude of the eigenvector is always positive and never goes exactly to zero. This shortcoming is illustrated in Fig. 1. There is a well-defined minimum near $\bar{\omega} = 0.35$; however, ambiguous secondary minima exist near $\bar{\omega} = 0.43$ and 0.46. It cannot be discerned with certainty which of these features represents the actual flutter condition.

The results of Kholodar et al. [1] for the NACA 64A010 airfoil were used as a benchmark case to ensure that this method produced correct results. In general, results from the minimum magnitude solution agreed with Kholodar et al.'s. A curious outcome, however, was the evidence of potential multiple solutions to Eq. (5), such as those indicated in Fig. 1. These multiple solutions were concentrated in a range of Mach numbers from $M = 0.84$ to 0.9. Kholodar et al.'s findings showed a single point at each Mach number for the edge of the flutter boundary. In an effort to determine why these additional solutions were occurring, a second numerical method for solving $\det(E) = 0$ was developed.

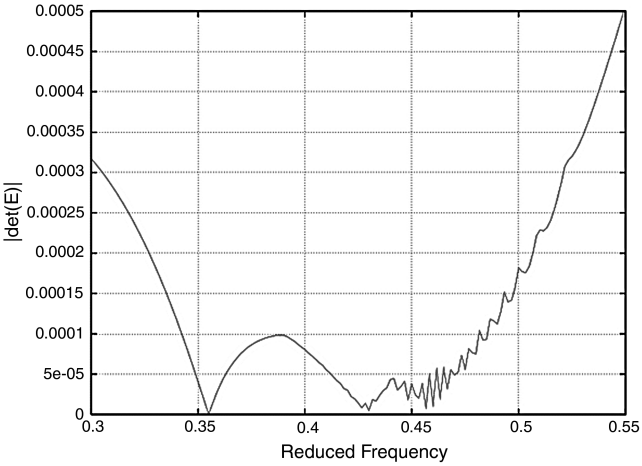

Fig. 1 Determinant magnitude as a function of $\bar{\omega}$ using the minimum magnitude approach; $M = 0.88$ and NACA 64A010 airfoil.

B. Bisection-Spline Method

Since the quantity $\det(E)$ is complex, interval bisection (or another nonlinear root-finding method) can be used to find the conditions that satisfy

$$\Re\{\det(E)\} = \Im\{\det(E)\} \tag{6}$$

The solutions of Eq. (6) are then examined for the specific conditions in which $\Re\{\det(E)\} = \Im\{\det(E)\} = 0$.

Use of the minimum magnitude method indicated the potential for multiple solutions to Eq. (6) at a given reduced frequency. A nonlinear root-finding method such as Newton's method or interval bisection converges on a single root. In order to find all roots, a modified bisection method was used. This method first evaluates the difference $\Re\{\det(E)\} - \Im\{\det(E)\}$ at discrete intervals of V and looks for sign changes in the result. When a sign change occurs, bisection is begun on the interval to find the exact reduced velocity and frequency of the zero crossing. The size of the discrete interval at which this difference is evaluated must be tuned to the nature of the particular function. Although any root-finding method would have worked, bisection was chosen for its straightforwardness of implementation.

To find the reduced velocity and reduced frequency at flutter, it was originally thought that two reduced frequencies could be picked, one above the flutter reduced frequency and one below. For each frequency, the reduced velocity satisfying Eq. (6) could be computed via interval bisection or another nonlinear root-finding method. Then, via linear interpolation, an approximation to the flutter reduced velocity would be made. In practice, it was found that linear interpolation failed to identify a solution; when different frequencies were used, the reduced velocity at solution was also different.

Rather than discarding this approach, a cubic spline was fit to the aerodynamic lift and moment input data. Then the interpolated aerodynamic data were passed to the modified bisection algorithm finding all solutions of Eq. (6). A plot of reduced velocity versus $\Re\{\det(E)\}$ [which is equal to $\Im\{\det(E)\}$ for all solutions of Eq. (6)] was generated. Examples of these plots are shown later.

The flutter reduced velocity was then extracted from such plots by connecting the data points with smooth curves and looking for the intersections of the curves with a line drawn through $\Re\{\det(E)\} = 0$. This method was also implemented as a C++ code, using gnuplot for

visualization and the GNU plotutils package for fitting of cubic splines.

This method produced results that agreed with those of the minimum magnitude solution method. But it also offered greater insight into the nature of the multiple solutions observed.

C. Multiple Solutions in the Inviscid Case

Figure 2 shows a typical single crossing with $\Re\{\det(E)\} = 0$, indicating a single flutter velocity. However, a surprising result was that for Mach numbers in the range of $M = 0.84$ to 0.9, multiple crossings were present, as shown in Fig. 3. As seen in Figs. 4 and 5, these plots could be constructed either in terms of the reduced velocity V or the reduced frequency $\bar{\omega}$, with the same roots occurring in either case. The few outlier points seen in the plots are an artifact of the particular postprocessing algorithm used.

The bisection-spline method presented a means to categorize these multiple roots as well. In each multiple-root case, one root was approached by increasing the value of $\Re\{\det(E)\}$, another was approached by decreasing $\Re\{\det(E)\}$, and the third was bracketed between these two. Henceforth, these will be referred to as the $-$ side, $+$ side, and middle roots, respectively. When the results over a range of Mach numbers were collected, these groups of roots formed families of solutions. For example, all of the $+$ side roots formed a distinct, simply connected branch. The same was true for the other two kinds of roots. Kholodar et al.'s [1] solution, which also used inviscid aerodynamics, matched these findings and presented what turned out to be a subset of these solution families. However, this analysis did not note the occurrence of multiple solutions.

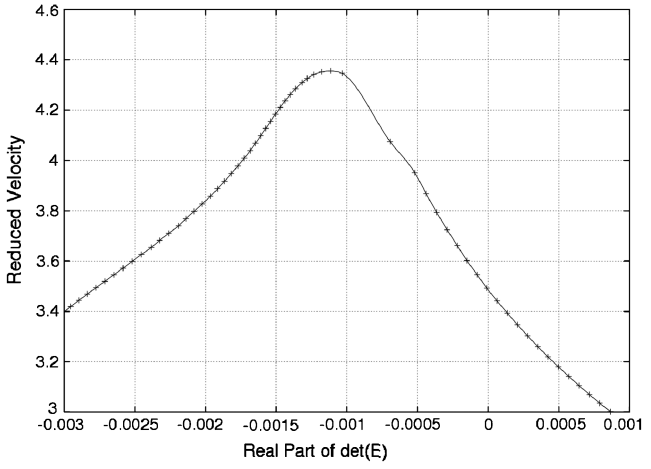

Fig. 2 Example of root behavior for a flutter solution with a single root present; $M = 0.80$ and NACA 64A010 airfoil.

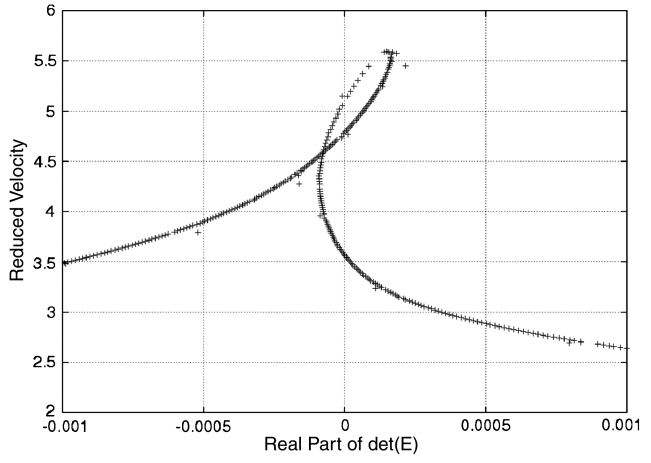

Fig. 3 At a higher Mach number, multiple solutions occur when using the inviscid model; $M = 0.88$ and NACA 64A010 airfoil.

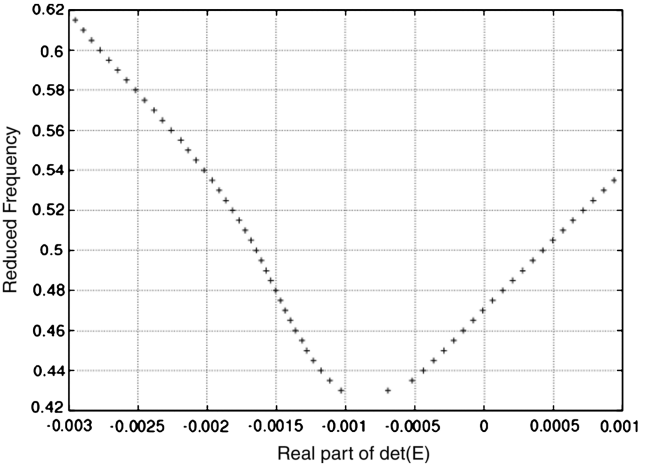

Fig. 4 Single-root flutter solution shown in terms of reduced frequency; $M = 0.80$ and NACA 64A010 airfoil.

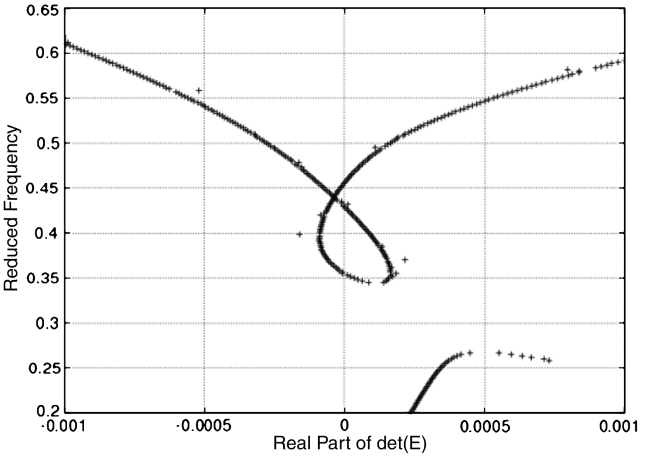

Fig. 5 Multiple-root flutter solution expressed in terms of reduced frequency; $M = 0.80$ and NACA 64A010 airfoil.

Unlike the minimum magnitude method, the bisection-spline method offers both a more definite prediction in the region with multiple solutions at a given V and a means to group these solutions into families.

IV. Comparison with Previous Computational Results for NACA 64A010 Airfoil

Both the minimum magnitude and bisection-spline methods were used to successfully reproduce the inviscid flutter boundary calculated by Kholodar et al. [1] for the NACA 64A010 airfoil used as a test case.

A. Inviscid Results

In the inviscid calculation, both methods recovered Kholodar et al.'s [1] findings but also found additional solutions in a region from $M \approx 0.84$ to ≈ 0.90. Using the bisection-spline method, it was observed that these additional solutions form an enclosed region, as noted in Figs. 6a and 6b. As any solution of Eq. (6) is a point of neutral stability to the governing equations, the authors postulate that after crossing the lowest part of the flutter boundary, the system goes unstable. Then, when it enters the small enclosed region, it enters a weakly stable regime. If the reduced velocity is increased further, the system exits the regime and becomes unstable again. Thus, it is thought that the enclosed region is weakly stable.

The region is not likely to be physically meaningful, however, since introducing a small amount of structural damping to the system causes the additional solutions to disappear. The remaining solution agrees exactly with that found by Kholodar et al.[1]. The structural

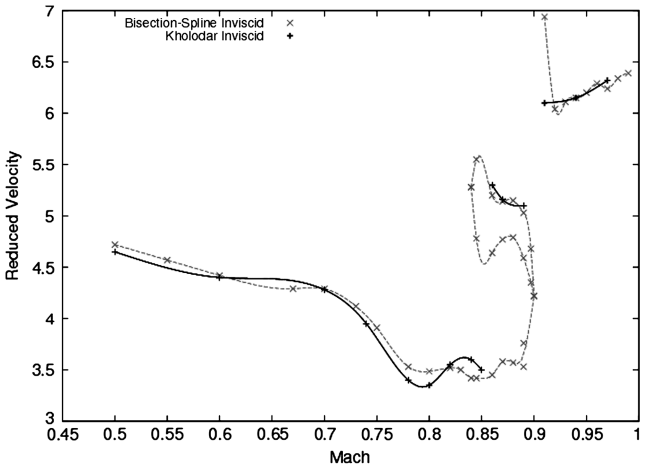

a)

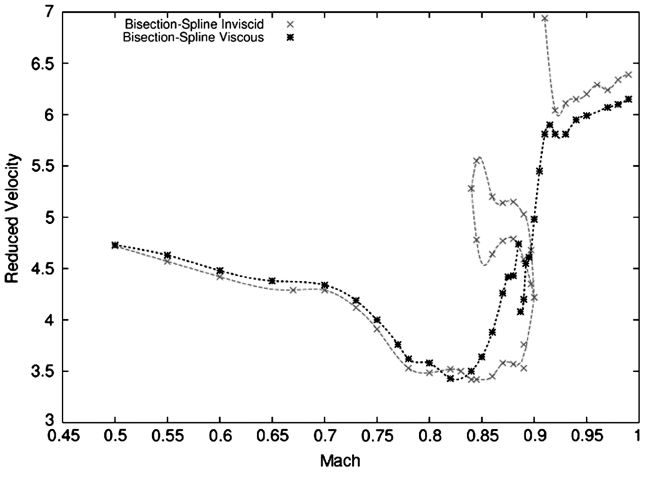

b)

Fig. 6 Plots of a) inviscid results via the bisection-spline method compared with those of Kholodar et al. [1] (NACA 64A010 airfoil) and b) results for inviscid and viscous aerodynamic models via the bisection-spline flutter boundary prediction method (NACA 64A010 airfoil).

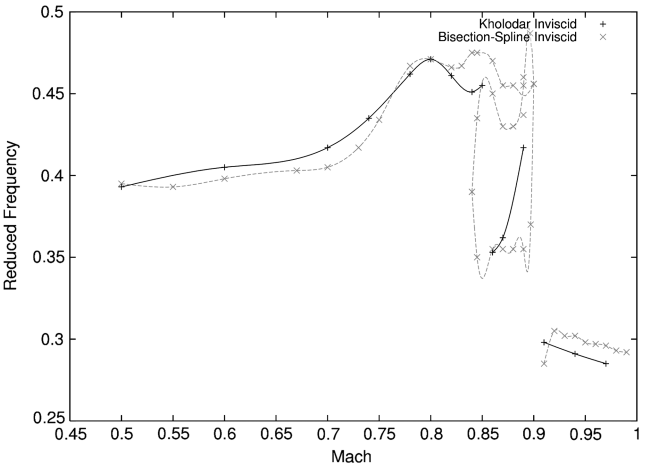

a)

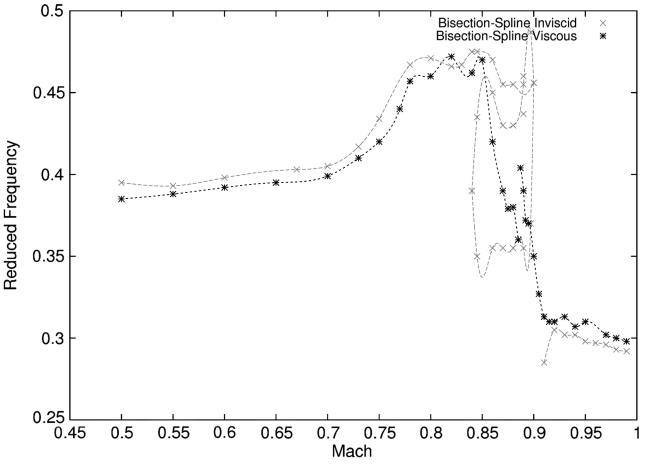

b)

Fig. 7 Plots of a) calculated flutter $\bar{\omega}$ versus M obtained via the bisection-spline method compared with the results of Kholodar et al. [1] (NACA 64A010 airfoil) and b) comparison of inviscid and viscous results for flutter $\bar{\omega}$ found via the bisection-spline method (NACA 64A010 airfoil).

damping was introduced by adding a damping coefficient ig to the diagonal terms of the structural matrix. Thus, Eq. (5) becomes

$$\det(E) = \left| -\bar{\omega}^2 \begin{pmatrix} 1 & x_\alpha \\ x_\alpha & r_\alpha^2 \end{pmatrix} + \frac{4}{V^2} \begin{pmatrix} \omega_h^2/\omega_\alpha^2 + ig & 0 \\ 0 & r_\alpha^2 + ig \end{pmatrix} - \frac{4}{\pi\mu} \begin{pmatrix} -\frac{1}{2}\frac{d\bar{c}_l}{dh} & -\frac{1}{2}\frac{d\bar{c}_l}{d\alpha} \\ \frac{d\bar{c}_m}{dh} & \frac{d\bar{c}_m}{d\alpha} \end{pmatrix} \right| = 0 \tag{7}$$

Although multiple flutter solutions are mathematically possible, physically, one mode dominates. Around $M = 0.9$, the system transitions to another flutter mode entirely, and the flutter reduced velocity increases substantially. For these calculations, $g = 0.04$ was chosen.

Figure 7a shows the predicted flutter reduced frequencies via the bisection-spline method and as obtained by Kholodar et al.[1]. As in the case of reduced velocity, the results are comparable up to the region near $M = 0.84$, where the enclosed weakly stable region begins.

B. Viscous Results

A key goal of this study was to quantify the influence of viscosity on the predicted flutter boundary. As depicted in Figs. 6b and 7b, the effects of viscosity are negligible at Mach numbers less than $M \approx 0.7$, and the consequences of viscosity remain moderate over most of the flow regime.

However, viscous effects play a critical role in the region from $M \approx 0.84$ to ≈ 0.90, where the inviscid flutter analysis revealed a weakly stable region within the flutter boundary, as shown in Fig. 6a. This feature is not observed in the viscous case. However, a region of sensitivity to Mach number occurs near $M = 0.88$, as shown in greater detail in Fig. 8. The authors conjecture that this sensitivity is

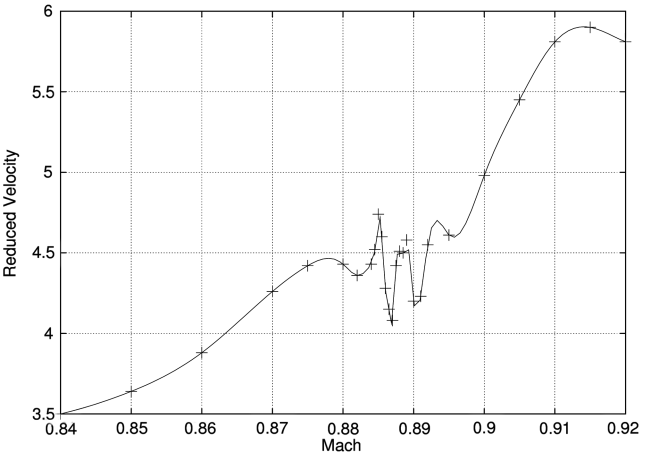

Fig. 8 Viscous results for the flutter boundary show a region of extreme sensitivity to Mach number in the range $0.87 < M < 0.90$ (NACA 64A010 airfoil).

the result of shock/boundary-layer interactions across the airfoil specific to this Mach number range and airfoil geometry.

Using the viscous HB flow solver, Mach number contours over the airfoil were visualized for several points in the transonic regime. As Fig. 9 indicates, at lower freestream Mach numbers, the flow over the entire airfoil is subsonic. As the airfoil enters the transonic range, a normal shock appears on the aft portion of the airfoil. As the Mach number is advanced further, the normal shock moves further aft on the airfoil and transitions to an oblique shock. It is believed that this shock transition, which occurs near $M = 0.88$, and its corresponding effect on shock-induced separation create the great sensitivity of the flutter boundary to Mach number over that same region.

The transition to an entirely new flutter mode near $M = 0.9$ appears to be a result of the shock on the airfoil transitioning from a normal shock to an oblique one. This results in a much smaller region of flow separation over the airfoil. The normal shock, on the other hand, creates a more separated flow and leads to another flutter mode. Where the transition from normal to oblique shock occurs, the flutter mode is also in transition and is consequently highly sensitive to Mach number.

Inviscid Mach number contours were also examined and were found to be very similar in visual appearance to those obtained when viscosity was included, except that boundary-layer effects were absent. The effects of viscosity, although subtle, still prove to be important in the transonic range.

V. Comparison with Wind-Tunnel Results for Benchmark Active Controls Technology NACA 0012 Airfoil

Previous computational studies by Kholodar et al. [1] tried to match the flutter boundary obtained experimentally by Rivera et al. [2] in the Transonic Dynamics Tunnel at NASA Langley Research Center as part of the Benchmark Active Controls Technology (BACT) program [5]. This experiment used a three-dimensional wing model with a constant-chord NACA 0012 section. The structural parameters were $x_\alpha = 0$, $r_\alpha^2 = 1.024$, $a = 0$, and $\omega_h/\omega_\alpha = 0.646$.

Kholodar et al.'s [1] inviscid calculation agreed very well with the experimental findings, except from $M \approx 0.88$ to ≈ 0.95 near what was termed a "plunge instability region" [2]. It was originally thought that including viscosity in this calculation might yield better agreement in the plunge instability region, motivating this current research.

Ashley [6] noted that the transition from frequency coalescence flutter to single-degree-of-freedom flutter is a consequence of formation of shocks on the airfoil. Using tufts to visualize the flowfield, Rivera et al. [2] observed substantial separation occurring in the plunge instability region. The plunge instability region observed thus appears to be dominated by shock-induced flow separation.

Experimental data for the flutter boundary were not obtained at Mach numbers just below the plunge instability region. Using an inviscid aerodynamic model in the flutter calculations, no flutter solutions could be obtained for $0.82 < M < 0.92$ except at very low flow densities (inverse mass ratios). This is approximately the same region for which experimental results were unavailable. Kholodar et al. [1] conjectured that this indicated that in this region, the flutter mass ratio (inversely proportional to flow density or dynamic pressure) rose precipitously as the airfoil entered a single degree-of-freedom flutter mode. Conversely, flow density (or inverse mass ratio) dropped precipitously.

Applying the bisection-spline flutter method and CFD models to this problem, the inviscid CFD results obtained agreed exactly with Kholodar et al.'s [1]. Furthermore, use of the method confirmed Kholodar et al.'s conjecture that flutter mass ratio increases

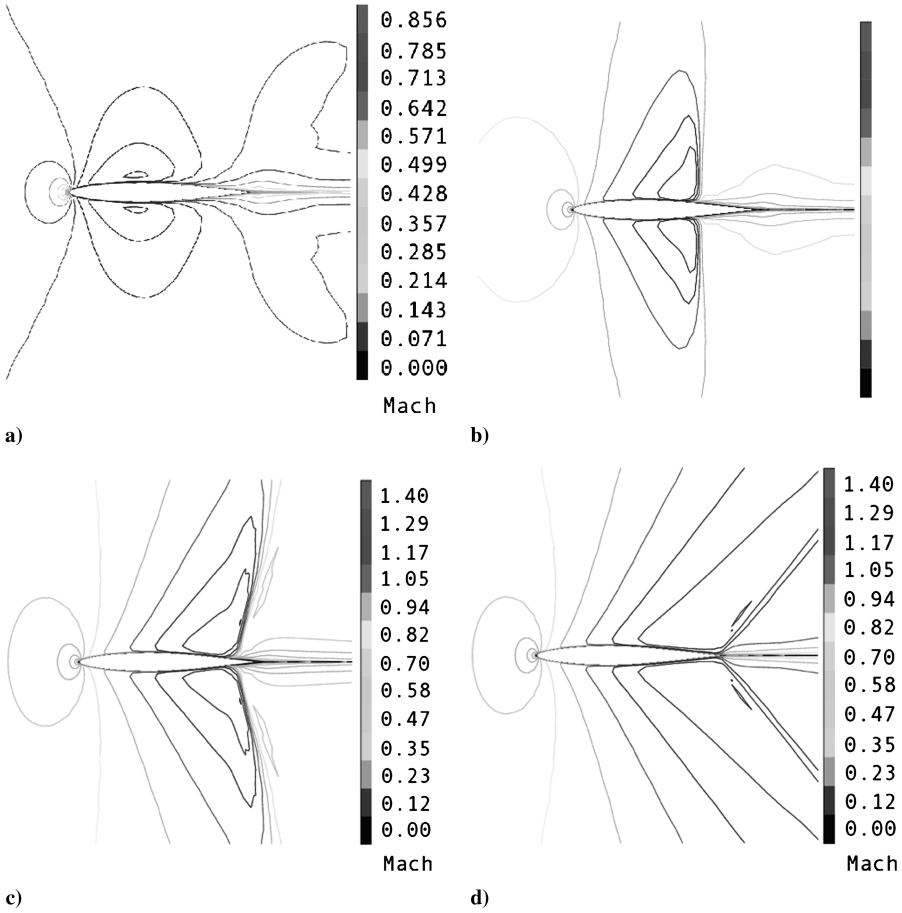

Fig. 9 Viscous prediction of Mach number contours in several flow regimes, NACA 64A010 airfoil: a) $M = 0.70$, b) $M = 0.84$, c) $M = 0.88$, and d) $M = 0.95$. The steady flow at zero angle of attack is shown.

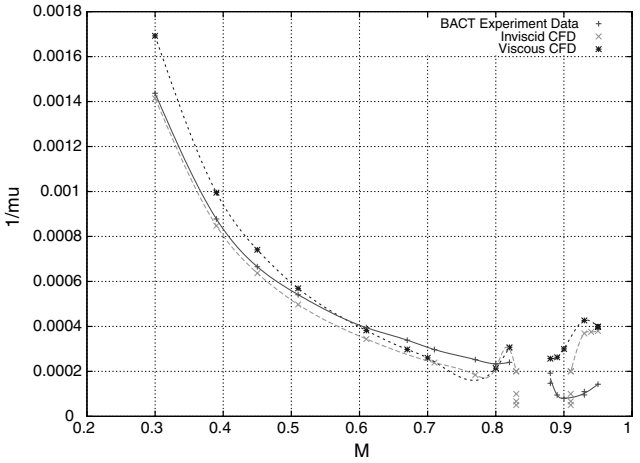

Fig. 10 Flutter boundary predicted using inviscid and viscous CFD models in conjunction with bisection-spline method and experimental result from Rivera et al. [2] (NACA 0012 airfoil).

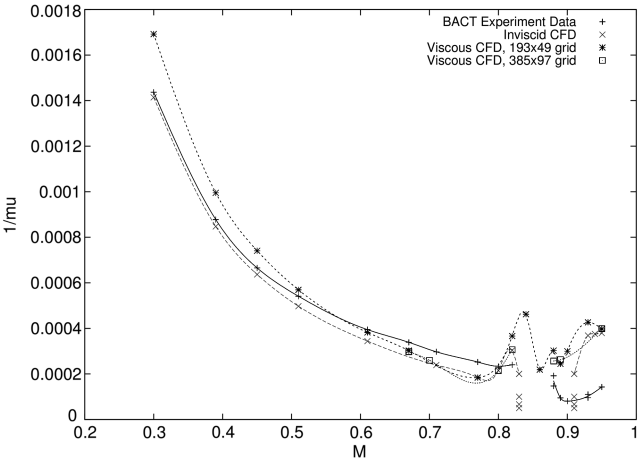

Fig. 12 Flutter mass ratio calculated using the 193 × 49 and 385 × 97 viscous grids, compared with inviscid CFD result and experimental data from Rivera et al. [2].

dramatically for $0.82 < M < 0.92$ (hence, inverse mass ratio decreases dramatically), as seen in Fig. 10.

This was determined by specifying the mass ratio and finding several Mach numbers at which the real and imaginary parts of $\det(E)$ were equal, via the bisection-spline method. Fitting a spline to these data, it was possible to infer the approximate flutter Mach number without running the flow solver at that Mach number specifically. In all, some 27 Mach numbers were surveyed in order to develop a complete representation of the flutter boundary.

Surveying several mass ratios, it was found that for $0.83 \leq M \leq 0.91$, the system fluttered even for extremely large mass ratios or correspondingly low flow density or dynamic pressure. The graphical result of these computations is shown in Fig. 11.

A. Viscous CFD Results

Viscous CFD results revealed a number of surprising characteristics. First, whereas inviscid aerodynamics made flutter solutions difficult to find in the region $0.83 \leq M \leq 0.91$ due to the sharp increase in flutter mass ratio μ, by contrast, viscous results on a 193×49 grid yielded readily detectable solutions. However, these viscous solutions showed some sensitivity to Mach number, similar to the sensitivity observed for the NACA 64A010 airfoil at comparable Mach numbers (recall Fig. 8).

1. Grid Refinement Study

A grid refinement study was performed to verify the results obtained on the nominal 193×49 grid. The flutter condition was recomputed on a coarser 97×25 grid and also a fine 385×97 grid at select Mach numbers, chosen to be representative of the range of Mach numbers examined. This study showed that the coarse 97×25 grid had insufficient resolution and produced results in poor agreement with experiment at low subsonic as well as transonic Mach numbers.

Results on the 385×97 computational mesh agreed with those on the nominal 193×49 mesh except for a narrow range of transonic Mach numbers. For $M \approx 0.84$–0.86, computations on this mesh showed flow shedding to be occurring: a phenomenon not seen on the coarser meshes. The range in which this shedding occurred agrees very closely with the Mach number range for which experimental results were not obtained: approximately $0.82 < M < 0.88$. As seen in Fig. 12, predictions on the 193×49 and 385×97 viscous grids largely agreed outside of this shedding region.

Shedding prohibits a linear flutter analysis at the Mach numbers for which it occurs, because it violates the assumption that the flow behaves in a dynamically linear way for small motions of the airfoil. Still, the present calculation provides an insight into the original flutter experiment. The occurrence of shedding correlates with the range of Mach numbers for which airfoil motions became erratic in the experiment, indicating that shedding may have led to this behavior.

2. Results for the Flutter Boundary

A composite flutter boundary has been compiled using data from the 193×49 mesh for Mach numbers outside the shedding region and the 385×97 mesh for the shedding region. The 385×97 mesh's high cell count causes an order-of-magnitude increase in

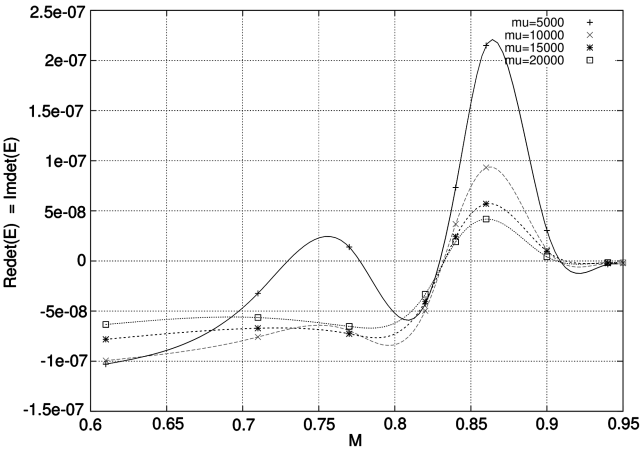

Fig. 11 For $0.83 \leq M \leq 0.91$, the inviscid flutter calculation predicts the model to flutter even for very large μ (NACA 0012 airfoil).

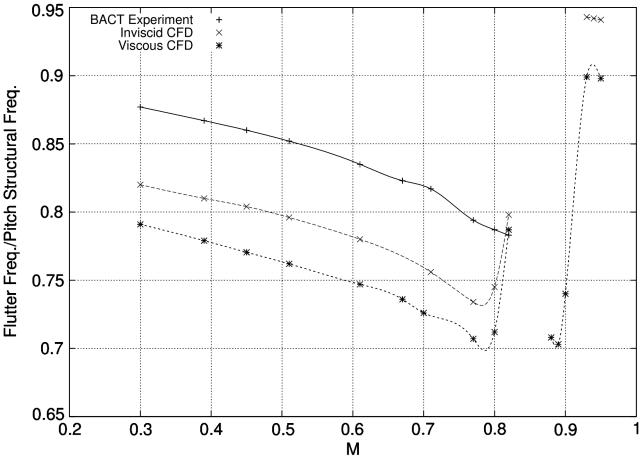

Fig. 13 Flutter frequency predicted using CFD models and experimental result from Rivera et al. [2].

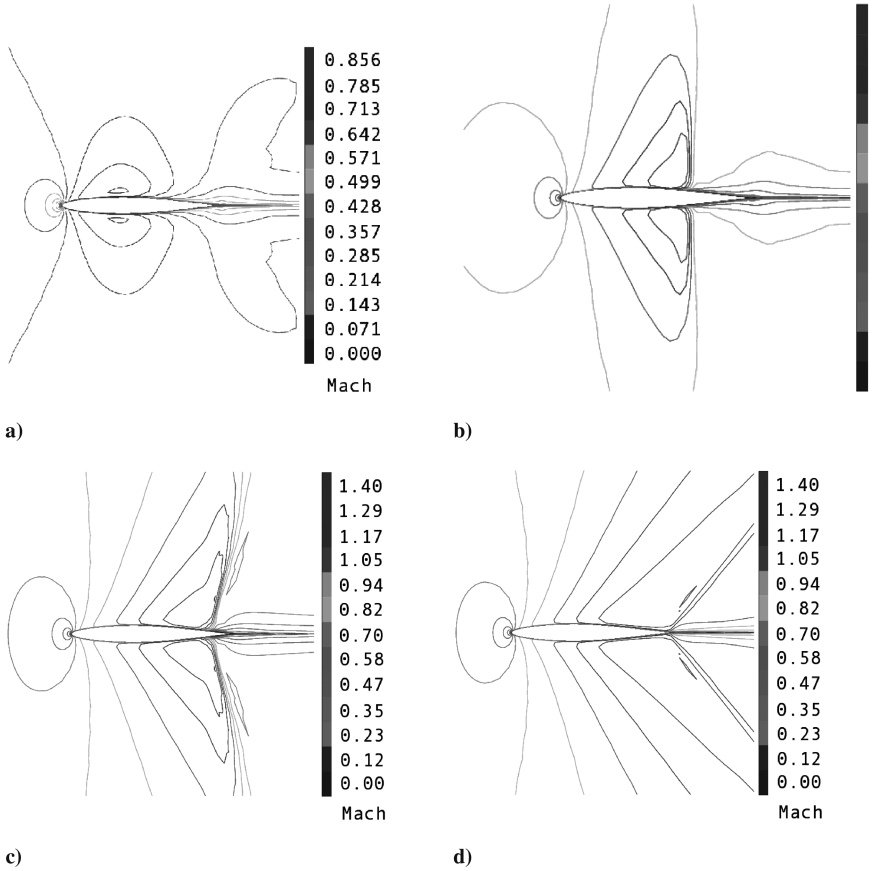

Fig. 14 Effect of Mach number on shock structure and shock-induced separation, NACA 0012 airfoil: a) $M = 0.82$, b) $M = 0.84$, c) $M = 0.88$, and d) $M = 0.92$. The steady flow at zero angle of attack is shown.

computation time, so it is advantageous to use the coarser mesh when it provides sufficient resolution. The composite viscous prediction of the flutter boundary in terms of $1/\mu$ vs M is shown in Fig. 10. Although agreement between computation and experiment is good over the conventional flutter boundary, the computational models fail to capture the experimental behavior in the plunge instability region, $M \geq 0.88$.

Results were also obtained for flutter frequency, as shown in Fig. 13. The same general trends as in the case of flutter mass ratio were observed. For $M \leq 0.82$, viscous and inviscid CFD predictions had the same trend and were close to the experimental results. Inside the plunge instability region, $0.88 \leq M \leq 0.95$, viscous and inviscid models roughly agreed but failed to match experimental results. These models show the flutter frequency increasing significantly within this flow regime.

Flow over the airfoil was computationally visualized at several representative Mach numbers, as seen in Fig. 14. For $M < 0.8$, flow over the airfoil is entirely subsonic. As the Mach number increases, a normal shock appears on the airfoil near midchord. The shedding region appears coincidentally with this normal shock, and it is thought that a shock/boundary-layer interaction over a narrow range of Mach numbers creates the conditions necessary for shedding to occur. By $M = 0.92$, the shock has transitioned to an oblique trailing-edge shock and shock-induced separation is greatly reduced.

B. Dynamic Pressure Results

The flutter boundary was also computed in terms of dynamic pressure and compared with experimental data. Dynamic pressure is obtained via the compatibility relation:

$$V \equiv U\frac{1}{\omega_\alpha b} = M\sqrt{\frac{T}{T_0}}\frac{a_0}{\omega_\alpha b} \tag{8}$$

Using tabulated values of T/T_0 as a function of M and with a known value for the flutter mass ratio, this relation can be solved to obtain the dynamic pressure based on U.

Figure 15 shows the experimentally observed flutter dynamic pressure, characterized by the trend of increasing flutter dynamic pressure up to $M = 0.82$. For $0.88 \leq M \leq 0.95$, in the plunge instability region, flutter dynamic pressure is seen to dip sharply. Here, a chimney of rapidly dropping q_f values is observed to fall sharply. These low values then recover by $M = 0.95$.

Computational models have difficulty matching the experimental results at transonic Mach numbers. CFD results, as shown in Fig. 15, fail to capture behavior in the plunge instability region entirely. Both inviscid and viscous calculations also fail to match the trend of

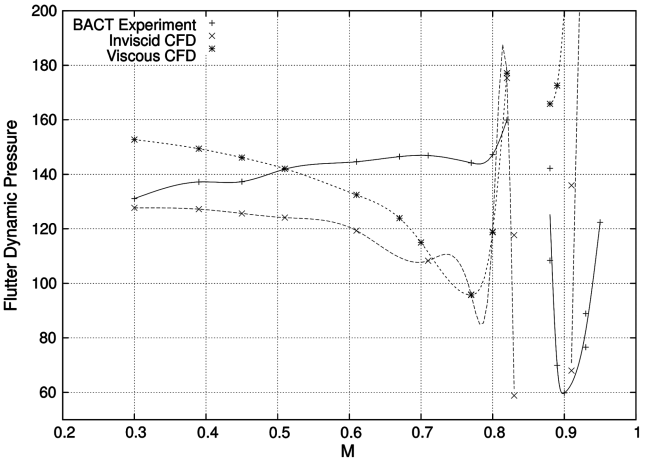

Fig. 15 CFD prediction of flutter dynamic pressure and experiment (focusing on values near experimentally predicted flutter boundary).

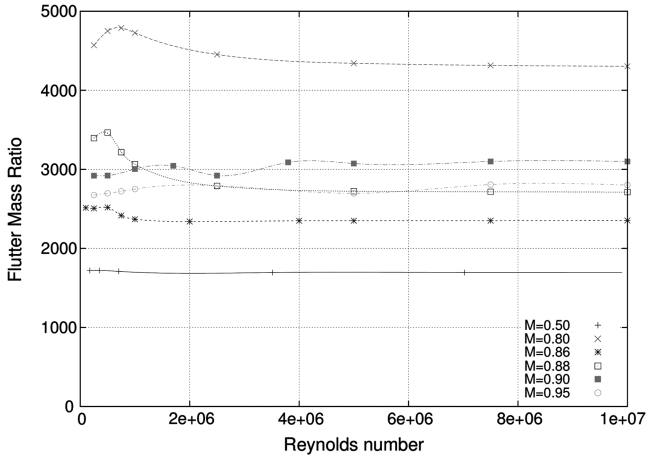

Fig. 16 Sensitivity of viscous flutter solutions to Reynolds number.

increasing q_f with Mach number, despite being generally of the correct order of magnitude.

C. Sensitivity of Results to Reynolds Number

Viscous flutter calculations were matched to the Reynolds numbers cited in the BACT test report [2]. However, since no experimental data were obtained for $0.82 < M < 0.88$, the Reynolds numbers used in computational analyses for this region were estimated based on the Reynolds number values at the region's boundaries.

To quantify the effects of Reynolds number variation on the solution, flutter solutions for several representative Mach numbers were calculated over a range of Reynolds numbers. Figure 16 shows the results of these calculations.

For cases outside the pitch–plunge instability region, such as at $M = 0.50$, the Reynolds number has little effect on the resulting flutter mass ratio. At greater Mach numbers, the Reynolds number has a subtle effect on the shock structure that appears on the airfoil.

For Mach numbers in the plunge instability region, the trends are similar. A very low Reynolds number leads to prediction of flutter at larger mass ratios. The most profound variation occurs for $M = 0.88$, where the flutter mass ratio varies from a median value by approximately $\pm 10\%$. Hence, sensitivity to Reynolds number is not a significant consideration for the BACT NACA 0012 case.

VI. Conclusions

An inviscid aerodynamic model is sufficient for the prediction of the flutter boundary of an isolated airfoil in most flow regimes. However, as the Mach number enters the transonic range, shock-induced separations have a significant effect on flutter boundary predictions. As separation cannot be accounted for in an inviscid aerodynamic model, it is recommended that a viscous model with increased grid density be used in this regime. At Mach numbers below $M = 0.7$ for the airfoils studied here, an inviscid flow solver provides reliable results along with a significant reduction in computational expense.

Use of a viscous aerodynamic computational model with a greatly refined grid showed that the flow may encounter shedding for a narrow range of Mach numbers, $0.82 < M < 0.88$. This region lies on the lower edge of the plunge instability region previously identified by Rivera et al [2]. This shedding region coincides with the range for which no wind-tunnel results were obtained. This is thought to indicate that the flow behavior changes substantially in this region, making it difficult to identify the flutter onset condition experimentally.

Critically, this shedding region was identified only on a greatly refined mesh, underscoring the subtlety of the flow physics in this Mach number range.

This two-dimensional aerodynamic model still fails to capture certain aspects of the experimentally observed flutter boundary. For example, the quantitative agreement between theory and experiment for the flutter boundary at higher Mach numbers within the plunge instability region is not satisfactory.

Future work will focus on use of a three-dimensional aerodynamic model to study whether 3-D effects are responsible for this difference in predicted and measured behavior of the flutter boundary at transonic Mach numbers. Wind-tunnel wall effects may also require investigation. The shedding region will require a separate analysis using tools to handle its flow nonlinearities, such as simulation using a time-accurate flow model or an extension of frequency-domain methods to include incommensurate frequencies.

References

[1] Kholodar, D., Dowell, E., Thomas, J., and Hall, K., "Limit-Cycle Oscillations of a Typical Airfoil in Transonic Flow," *Journal of Aircraft*, Vol. 41, No. 5, 2004, pp. 1067–1072. doi:10.2514/1.618

[2] Rivera, J., Jr., Dansberry, B., Bennett, R., Durham, M., and Silva, W., "NACA0012 Benchmark Model Experimental Flutter Results with Unsteady Pressure Distributions," NASA, TM 107581, 1992.

[3] Thomas, J., Dowell, E., and Hall, K., "Modeling Viscous Transonic Limit-Cycle Oscillation Behavior Using a Harmonic Balance Approach," *Journal of Aircraft*, Vol. 41, No. 6, 2004, pp. 1266–1274. doi:10.2514/1.9839

[4] Hall, K., Thomas, J., and Clark, W. S., "Computation of Unsteady Nonlinear Flows in Cascades Using a Harmonic Balance Technique," *AIAA Journal*, Vol. 40, No. 5, 2002, pp. 879–886. doi:10.2514/2.1754

[5] Abel, I., "Research and Applications in Aeroelasticity and Structural Dynamics at the NASA Langley Research Center," NASA Langley Research Center, TM 112852, Hampton, VA, 1997.

[6] Ashley, H., "The Role of Shocks in the 'Sub-Transonic' Flutter Phenomenon," *Journal of Aircraft*, Vol. 17, March 1980, pp. 187–197. doi:10.2514/3.57891